# Finite-Element Model Reduction of Surface-Mounted Permanent Magnet Machines by Exploitation of Geometrical Periodicity

M. Al Eit, S. Clenet, T. Henneron

# Finite-Element Model Reduction of Surface-Mounted Permanent Magnet Machines by Exploitation of Geometrical Periodicity

M. Al Eit, S. Clénet, and T. Henneron

Université de Lille, Arts et Metiers ParisTech, Centrale Lille, HEI, EA 2697–L2EP–Laboratoire d'Electrotechnique et d'Electronique de Puissance, F-59000 Lille, France

**This paper presents a methodology that allows taking advantage of the geometrical periodicity of electrical machines together with the modeling of rotor motion. It enables by means of the discrete Fourier transform (DFT) to reduce the large-scale system obtained from the finite-element model to several smaller independent subsystems, allowing a shortening of the computational time. Due to DFT properties, the computational time can be more reduced especially when we consider the inter-dependence of the spectral components under either balanced or unbalanced supply condition. In addition, a further reduction is possible in the case of balanced regimes where the distribution of the eventual numerical solution is governed by a limited number of prevailing harmonics.**

*Index Terms*— **Discrete Fourier transform (DFT), electromagnetic fields, finite-element (FE) analyses, geometrical periodicity, model reduction, rotating electric machines, surface-mounted permanent magnet (SMPM) machines.**

## I. Introduction

IN ELECTROMAGNETIC field computation, when the interaction between electric and magnetic variables cannot be solved analytically, solution by numerical techniques such as finite-element (FE) [1] or boundary element methods [2] are often used. When a fine mesh and a small time step are used, such numerical techniques lead usually to a substantial calculation time which prevents the intensive use of such model in a design process. To tackle this issue, model reduction techniques are widely used; they have shown their efficiency in reducing both computational time and memory storage requirements. Some of these model reduction techniques are based on the subdomain reduction, namely, the ones dealing with the perturbation principle [3], [4]; they are usually used to determine the solution only in the most relevant areas. Besides, other techniques are dealing with the order reduction of the equation system. Among these, we can mention the proper orthogonal decomposition [5], [6] which has proven its benefit in the electromagnetic simulation of numerical models with a very high number of unknowns. We can mention that there exist other approaches based on lookup table techniques that are widely used for an effective computational efficient in real time machine control and convertor design [7], [8]. In fact, all the foregoing mentioned approaches are classified under the *a posteriori* reduction techniques since they require initially, at least, one full model solution. However, in this paper, we are interested in *a priori* model reduction technique that deals with the exploitation of the geometrical periodicity [9]–[11] based on the discrete Fourier transform (DFT).

In a practical way, if an FE model presents a kind of magnetic symmetry due to a common periodicity between the geometry and the source distribution (permanent magnet and current density), it is common to take full advantage of it by meshing only a portion of the electromagnetic device yielding therefore to substantial calculation benefits. We can go further by using the group representation theory [9], [10], [12], [13] to take advantage of the geometrical symmetry even when the excitation sources do not share necessarily the same periodicity. This enables in the case of surface-mounted permanent magnet (SMPM) machines to reduce the mesh on a single section holding only one stator tooth.

To meet this objective in magnetostatic problems, this approach consists in constructing the full problem by duplicating the FE modeling of an elementary periodic cell. This elementary cell represents the smallest connected section that regenerates the complete model by a simple transformation. In this paper, we will not apply the group representation theory literally, but an equivalent approach based on the linear algebra theory and more particularly on the properties of the stiffness full FE model matrix which is in fact a block circulant matrix. By means of a DFT transformation, it has been shown in the linear case that we can reduce the original large FE problem to a series of independent subproblems with a reduced size [14], [15]. In the non-linear case, some techniques have been proposed to keep the block circulant property by using iterative algorithms based on the fixed-point technique or the transmission-line method. Such techniques allow not only to apply the DFT but also to account for the non-linearity by introducing an additional fictitious source term on the right-hand side of the equation system [11], [16].

In this paper, we present a methodology to construct a reduced model of an SMPM whose geometry enables to take full advantage of the previous approach in the linear case. First, the full FE model of an SMPM is detailed in Section II. In Section III, the reduction approach is presented, and a dedicated method to take into account the movement is introduced; the rotor motion is considered within the subproblems using the spatial Fourier interpolation method (SFIM) [17], [18] extended from the locked step method [19]. The dependence of Fourier components is also exploited to speed up the solution

of the problem. Furthermore, in a balanced supply regime, the source has a regular distribution, leading to a limited number of DFT dominant components. In such case, it is sufficient to solve only the corresponding subsystems. Finally, the proposed methodology is applied to the study of a nine teeth/eight poles SMPM example that does not present in fact any common symmetry between the pure geometric model and the source distribution.

## II. Finite-Element Modeling

In a domain $\Omega$ of boundary $\Gamma$ ($\Gamma = \Gamma_1 \cup \Gamma_2$ and $\Gamma_1 \cap \Gamma_2 = \{\}$), the magnetostatic equations and the associated constitutive medium relationship are

$$\nabla \times \vec{H} = \vec{J_s}, \quad \nabla . \vec{B} = 0 \tag{1}$$

$$\vec{H} = \nu \vec{B} - \nu \vec{B_r} \tag{2}$$

where $\vec{B}$ is the magnetic flux density vector, $\vec{H}$ is the magnetic field vector, $\vec{J_s}$ is the current source density vector, $\vec{B_r}$ is the residual magnetization vector in the permanent magnets, and $\nu$ is the reluctivity. To impose the uniqueness of the solution, boundary conditions are set on $\Gamma_1$ and $\Gamma_2$

$$\vec{H} \times \vec{n} = \vec{0} \quad \text{on } \Gamma_1; \quad \vec{B} . \vec{n} = 0 \quad \text{on } \Gamma_2 \tag{3}$$

with $\vec{n}$ the outward boundary unit normal vector.

To solve (3), the magnetic vector potential $\vec{A}$ ($\vec{B} = \nabla \times \vec{A}$) is used. Besides, to ensure the unicity of $\vec{A}$, we most often add the Coulomb gauge which is, however, implicitly verified in the case of 2-D modeling. The resulting vector potential formulation from (1) and (2) is now given by

$$\nabla \times \nu(\nabla \times \vec{A}) = \nabla \times \nu \vec{B_r} + \vec{J_s}. \tag{4}$$

In the following, we will clarify how to exploit the geometrical periodicity of the structure of an electrical machine. We consider, therefore, as an example, an SMPM consisting of nine stator teeth supporting a three-phase winding and eight rotor poles (Fig. 1). Due to the non-consistent periodicity between stator and rotor sources, this machine does not present effectively any magnetic symmetry. However, it presents a periodicity that holds on the material permeability, i.e., the geometry regardless of the source distribution (current and residual magnetic flux densities). Therefore, in this machine case, we can discern nine identical cells in space. The principle of the determination of the elementary periodic cell is given in Fig. 1: concerning only the permeability of the materials, this elementary cell is defined by a machine section involving a single stator tooth.

To generalize, let us consider now the case of an electromagnetic device made up of $N$ periodical sections in space (Fig. 2). We suppose that the periodicity holds only on the permeability but not on the sources produced by the currents or the residual magnetic flux density.

We admit that all the sections are discretized by the same mesh and have thus the same number and distribution of nodes. Therefore, it can be shown that it is sufficient to model only an elementary section, as the one presented in Fig. 2, in such a way that the complete model can be deduced by a simple

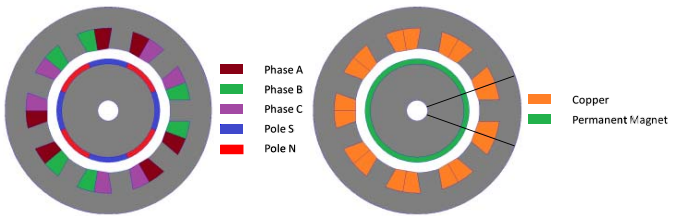


Fig. 1. 9/8 synchronous machine: highlighting different sources (left) and considering the permeability of materials regardless of sources (right).

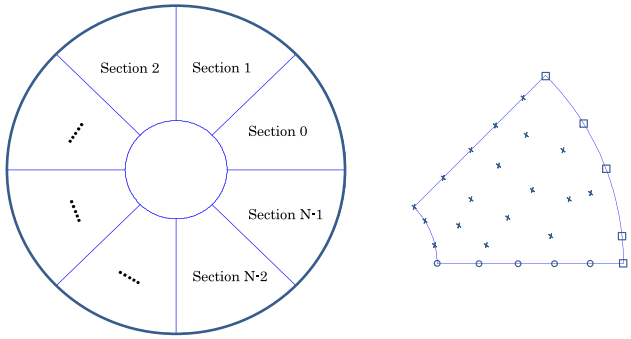


Fig. 2. Full model (left). Modeling of one elementary section: the crossed points represent the inner nodes, the round points represent the ones common with the previous section, and the squared points represent the ones subjected to Dirichlet conditions (right).

duplication of this elementary model. In each section, $n$ is supposed to be the number of degrees of freedom. It represents the total number of inner nodes excepting: i) the ones on the boundary where a Dirichlet condition is imposed and ii) the ones on the common side with the previous section of the device (see Fig. 2).

Taking into account now the periodicity on the material characteristics of the $N$ sections, the 2-D FE formulation of the linear magnetostatic problem, given in (4), leads to the following matrix system to solve:

$$\begin{pmatrix} S & S' & 0 & \cdots & 0 & S'' \\ S'' & S & S' & 0 & \cdots & 0 \\ \cdots & \cdots & \cdots & \cdots & \cdots & \cdots \\ \cdots & \cdots & \cdots & \cdots & \cdots & \cdots \\ \cdots & \cdots & \cdots & \cdots & \cdots & \cdots \\ \cdots & \cdots & \cdots & \cdots & \cdots & \cdots \\ S' & 0 & \cdots & 0 & S'' & S \end{pmatrix} \begin{pmatrix} A_0 \\ A_1 \\ \vdots \\ \vdots \\ \vdots \\ \vdots \\ A_{(N-1)} \end{pmatrix} = \begin{pmatrix} F_0 \\ F_1 \\ \vdots \\ \vdots \\ \vdots \\ \vdots \\ F_{(N-1)} \end{pmatrix} \tag{5}$$

$$[S_c][A] = [F] \tag{6}$$

where $[S_c]$ is a block circulant matrix of the full FE model, $[A]$ of size $([N \times n] \times 1)$ is the set of unknown nodal magnetic potential, and $[F]$ is the source term. $[S]$ of size $(n \times n)$ is the matrix accounting for the inner contribution of each section $i$, $[S'']$ is the matrix accounting for the contribution on the section $i$ of the previous section $i-1$, and $[S']$ is the matrix accounting for the contribution on the section $i$ of the next section $i+1$. $[A_i]$ and $[F_i]$ of size $(n \times 1)$ are, respectively, the set of unknown nodal magnetic potential and the source term calculated in the section $i$ $(0 \leq i \leq N-1)$.

## III. Model Reduction Methodology

### A. Model Reduction at a Fixed Rotor Position

Using a DFT, the block circulant matrix $[S_c]$ can be factorized under the following expression [5], [14], [20]:

$$[S_c] = [W][S_\Delta][W]^{-1}. \tag{7}$$

The matrix $[W]$ and the block diagonal matrix $[S_\Delta]$ will be given, respectively, as follows:

$$[W] = [U] \otimes [I_{dn}] \tag{8}$$

$$[S_\Delta] = \begin{pmatrix} S_{00} & 0 & \cdots & \cdots & \cdots & \cdots & 0 \\ 0 & S_{11} & 0 & \cdots & \cdots & \cdots & 0 \\ 0 & 0 & S_{22} & 0 & \cdots & \cdots & 0 \\ \vdots & \vdots & \vdots & \vdots & \vdots & \vdots & \vdots \\ \vdots & \vdots & \vdots & \vdots & \vdots & \vdots & \vdots \\ \vdots & \vdots & \vdots & \vdots & \vdots & \vdots & 0 \\ 0 & \cdots & \cdots & \cdots & \cdots & 0 & S_{(N-1)(N-1)} \end{pmatrix} \tag{9}$$

where $\otimes$ is the Kronecker product and $[I_{dn}]$ of size $(n \times n)$ is the identity matrix. The entries of the DFT matrix $[U]$ of size $(N \times N)$ are given in the following expression:

$$U(c,l) = \frac{1}{\sqrt{N}} e^{j\frac{2\pi}{N}(c-1)(l-1)}; \quad 1 \leq c \leq N \quad \text{and } 1 \leq l \leq N. \tag{10}$$

Combining now (6) and (7), we obtain

$$[W][S_\Delta][W]^{-1}[A] = [F]. \tag{11}$$

Multiplying the system (11) by the inverse matrix $[W]^{-1}$, we retreive the following new system to solve:

$$[S_\Delta][Z] = [C] \tag{12}$$

with

$$[Z] = [W]^{-1}[A] \quad \text{and } [C] = [W]^{-1}[F]. \tag{13}$$

Since $[S_\Delta]$ is a block diagonal matrix, we have, therefore, $N$ independent subsystems of size $n$ to be solved

$$[S_{ii}][Z_i] = [C_i]; \quad 0 \leq i \leq N-1. \tag{14}$$

The original system (6) of size $n \times N$ is now transformed into a set of $N$ independent subsystems of size $n$. From the solutions of these $N$ subsystems, the solution of the full model on the $N$ sections can be deduced from (13) and given by $[A] = [W][Z]$. Avoiding solving the full model system of dimension $n \times N$ by solving $N$ independent subsystems of dimensions $n$ each, leads effectively to a reduction in the computational time. The considered acceleration in the computational time is denoted $\gamma$ in the following.

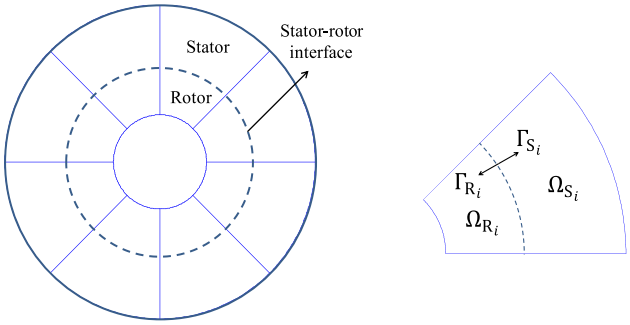


Fig. 3. Full model of a rotating electromagnetic device. The marked fictive interface separates the fixed part (stator) from the rotating part (rotor) (left). Modeling of one elementary section (right).

### B. Model Reduction Considering the Rotor Motion

In this section, we suppose the general case of a rotating electromagnetic device, consisting of a fixed stator and a movable rotor, and having a periodical structure as described in Section II. To the author's knowledge, no method combining the rotor movement and the DFT approach has been already proposed in the literature. However, such method is required to fully model such rotating electromagnetic device. To tackle this issue, the consideration of the rotor motion in this paper will be combined to our model reduction approach using the SFIM [17], [18] which is an extension of the locked step method [19]. To do so, the presence of a fictive interface between the stator and the rotor is defined (Fig. 3). Since the full model of the device represents $N$ identical sections in space, the geometrical periodicity, as it has been said before, can be exploited to simplify the model to only one elementary section.

In Fig. 3, we can notice that in each section $i(0 \leq i \leq N-1)$, we have the stator domain $\Omega_{si}$ whose number of degrees of freedom is $n_s$ and the rotor domain $\Omega_{ri}$ whose number of degrees of freedom is $n_r$. The stator–rotor interface, where the motion is taken into account, is duplicated to create dual $\Gamma_{si}$ and $\Gamma_{ri}$ separation interfaces which belong, respectively, to $\Omega_{si}$ and $\Omega_{ri}$. The relationship between the discretization nodes of the two interfaces $\Gamma_{si}$ and $\Gamma_{ri}$ allows, according to the locked step method [19] or the SFIM [17], [18], considering the rotor motion. When $m_D$ is the total number of nodes of the stator–rotor interface, we should denote that the number of degrees of freedom $n_g = m_D/N$, related to both interfaces $\Gamma_{si}$ and $\Gamma_{ri}$ in each section, is included, respectively, in both $n_s$ and $n_r$.

On the basis of the foregoing, we can summarize that there are $N$ periodic sections in the stator, the degree of freedom of each is $n_s$, and $N$ periodic sections in the rotor, and the degree of freedom of each is $n_r$. The use of the geometrical periodicity which makes it possible to construct the full model of the electromagnetic device by concatenation

of the elementary section model leads to obtain, according to (5) and (6); the following overdetermined system to be solved:

$$\begin{pmatrix} [S_{cS}] & [0] \\ [0] & [S_{cR}] \end{pmatrix} \begin{pmatrix} [A_{\mathrm{SS}}] \\ [A_{\mathrm{RR}}] \end{pmatrix} = \begin{pmatrix} [F_{\mathrm{SS}}] \\ [F_{\mathrm{RR}}] \end{pmatrix} \tag{15}$$

where $[S_{cS}]$ and $[S_{cR}]$ are two block circulant matrices linked to stator and rotor geometrical domains, respectively. $[A_{\mathrm{SS}}]$ and $[A_{\mathrm{RR}}]$ which are, respectively, of size $([N \times n_s] \times 1)$ and $([N \times n_r] \times 1)$, represent the vectors of the magnetic potential unknowns, and $[F_{\mathrm{SS}}]$ and $[F_{\mathrm{RR}}]$ are the source terms. The vectors $[A_{\mathrm{SS}}]$, $[A_{\mathrm{RR}}]$, $[F_{\mathrm{SS}}]$, and $[F_{\mathrm{RR}}]$ are given with their following explicit forms:

$$[A_{\mathrm{SS}}] = \begin{pmatrix} A_{S0} \\ A_{\Gamma_{S0}} \\ A_{S1} \\ A_{\Gamma_{S1}} \\ \vdots \\ \vdots \\ A_{S(N-1)} \\ A_{\Gamma_{S(N-1)}} \end{pmatrix}; \quad [A_{\mathrm{RR}}] = \begin{pmatrix} A_{R0} \\ A_{\Gamma_{R0}} \\ A_{R1} \\ A_{\Gamma_{R1}} \\ \vdots \\ \vdots \\ A_{R(N-1)} \\ A_{\Gamma_{R(N-1)}} \end{pmatrix}$$

$$[F_{\mathrm{SS}}] = \begin{pmatrix} F_{S0} \\ F_{\Gamma_{S0}} \\ F_{S1} \\ F_{\Gamma_{S1}} \\ \vdots \\ \vdots \\ F_{S(N-1)} \\ F_{\Gamma_{S(N-1)}} \end{pmatrix}; \quad [F_{\mathrm{RR}}] = \begin{pmatrix} F_{R0} \\ F_{\Gamma_{R0}} \\ F_{R1} \\ F_{\Gamma_{R1}} \\ \vdots \\ \vdots \\ F_{R(N-1)} \\ F_{\Gamma_{R(N-1)}} \end{pmatrix} \tag{16}$$

where $[A_{\mathrm{SS}i}] = [A_{Si}, A_{\Gamma_{Si}}]^T$ represents the set of the total unknown nodal magnetic potential in the stator domain $\Omega_{si}$ of the section $i$. $A_{Si}$ represents the set of unknown nodal magnetic potential in the stator domain except the ones on the interface $\Gamma_{Si}$ which are represented by the vector $A_{\Gamma_{Si}}$. $[F_{\mathrm{SS}i}] = [F_{Si}, F_{\Gamma_{Si}}]^T$ is the source term calculated on the stator domain $\Omega_{si}$. $F_{Si}$ is the source term calculated on the stator domain but referring to the nodes belonging to the stator domain excepting those on the interface $\Gamma_{Si}$ whose associated source term is given by $F_{\Gamma_{Si}}$. As for the rotor terms $A_{\mathrm{RR}i}$, $A_{Ri}$, $A_{\Gamma_{Ri}}$, $F_{\mathrm{RR}i}$, $F_{Ri}$, and $F_{\Gamma_{Ri}}$, they are homologous to the previously defined stator terms $A_{\mathrm{SS}i}$, $A_{Si}$, $A_{\Gamma_{Si}}$, $F_{\mathrm{SS}i}$, $F_{Si}$, and $F_{\Gamma_{Si}}$.

$[S_{cS}]$ and $[S_{cR}]$ being block circulant matrices, they can be factorized separately under the following forms:

$$\begin{aligned} [S_{cS}] &= [W_S][S_{\Delta S}][W_S]^{-1} \\ [S_{cR}] &= [W_R][S_{\Delta R}][W_R]^{-1} \end{aligned} \tag{17}$$

where $[S_{\Delta S}]$ and $[S_{\Delta R}]$ are two block diagonal matrices and the transformation matrices $[W_s]$ and $[W_R]$ will be given, respectively, in terms of the DFT matrix $[U]$ as follows:

$$[W_S] = [U] \otimes [I_{dn_S}] \tag{18}$$

$$[W_R] = [U] \otimes [I_{dn_R}] \tag{19}$$

where $[I_{dn_S}]$ and $[I_{dn_R}]$ are the identity matrices of size $(n_S \times n_S)$ and $(n_R \times n_R)$, respectively.

Combining now the system (15) with (17), we obtain, in the harmonic domain, the new system to solve

$$\begin{pmatrix} [S_{\Delta S}] & [0] \\ [0] & [S_{\Delta R}] \end{pmatrix} \begin{pmatrix} [Z_{\mathrm{SS}}] \\ [Z_{\mathrm{RR}}] \end{pmatrix} = \begin{pmatrix} [C_{\mathrm{SS}}] \\ [C_{\mathrm{RR}}] \end{pmatrix} \tag{20}$$

where the vectors $[Z_{\mathrm{SS}}]$, $[Z_{\mathrm{RR}}]$, $[C_{\mathrm{SS}}]$, and $[C_{\mathrm{RR}}]$ will be given in the following expressions:

$$[Z_{\mathrm{SS}}] = [W_S]^{-1}[A_{\mathrm{SS}}] \quad \text{and } [C_{\mathrm{SS}}] = [W_S]^{-1}[\mathrm{F_{SS}}] \tag{21}$$

$$[Z_{\mathrm{RR}}] = [W_R]^{-1}[A_{\mathrm{RR}}] \quad \text{and } [C_{\mathrm{RR}}] = [W_R]^{-1}[F_{\mathrm{RR}}]. \tag{22}$$

Since $[S_{\Delta S}]$ is a block diagonal matrix, we have, therefore, $N$ independent overdetermined subsystems to solve, of size $n_S$ each, and since $[S_{\Delta R}]$ is a block diagonal matrix, we have likewise, therefore, $N$ independent overdetermined subsystems to solve, of size $n_R$ each

$$\begin{aligned} [S_{ii_{\Delta S}}][Z_{\mathrm{SS}i}] &= [C_{\mathrm{SS}i}]; \quad 0 \le i \le N-1 \\ [Z_{\mathrm{SS}i}] &= \begin{bmatrix} Z_{Si} \\ Z_{\Gamma_{Si}} \end{bmatrix}; \quad [C_{\mathrm{SS}i}] = \begin{bmatrix} C_{Si} \\ C_{\Gamma_{Si}} \end{bmatrix} \end{aligned} \tag{23}$$

$$\begin{aligned} [S_{jj_{\Delta R}}][Z_{\mathrm{RR}i}] &= [C_{\mathrm{RR}i}]; \quad 0 \le j \le N-1 \\ [Z_{\mathrm{RR}i}] &= \begin{bmatrix} Z_{Ri} \\ Z_{\Gamma_{Ri}} \end{bmatrix}; \quad [C_{\mathrm{RR}i}] = \begin{bmatrix} C_{Ri} \\ C_{\Gamma_{Ri}} \end{bmatrix}. \end{aligned} \tag{24}$$

To solve these different overdetermined independent subsystems in the stator and the rotor domains, they have to be coupled together, and thus we have to express different $[Z_{\Gamma_{Ri}}]$ as functions of different $[Z_{\Gamma_{Sj}}]$. In other words, where $[Z_{\Gamma_S}]$ and $[Z_{\Gamma_R}]$ are, respectively, the set of $[Z_{\Gamma_{Si}}]$ and $[Z_{\Gamma_{Ri}}]$, we have to express $[Z_{\Gamma_S}]$ as a function of $[Z_{\Gamma_R}]$.

In fact, in our case, the relationship between $[Z_{\Gamma_S}]$ and $[Z_{\Gamma_R}]$ is determined in such a way as to take into account the rotor motion. The latter is performed using the SFIM. It allows considering effectively any rotation angle $\theta$ and not only the discrete few angle steps given by $\theta_m = m\Delta\theta$, where $m \in \mathbb{Z}$ and $\Delta\theta$ is a previously fixed rotation angle step.

By this method, to take into account the continuous rotor motion, the vector assembling the nodes belonging to the interface solidary to the rotor $[A_{\Gamma_R}]$ is expressed as a function of that assembling the nodes of the interface solidary with the stator $[A_{\Gamma_S}]$. This is done by assuming that the DFT of both vectors are given in the following expression:

$$[Z_{F_{\Gamma_R}}] = [D(\theta)][Z_{F_{\Gamma_S}}] \tag{25}$$

where $[D(\theta)]$ is the diagonal matrix linking the DFT $[Z_{F_{\Gamma_R}}]$ of $[A_{\Gamma_R}]$ to the DFT $[Z_{F_{\Gamma_S}}]$ of $[A_{\Gamma_S}]$. It allows adding a phase lag of amplitude $\theta$ to a signal, by multiplying its $k$th harmonic by $e^{j\theta k}$. When $m_D$ is the total number of nodes of the stator–rotor interface, the entries of the matrix $[D(\theta)]$ of size $(m_D \times m_D)$ are given in the following expression [18]:

$$D(i,i) = \begin{cases} e^{j\theta(i-1)}; & i \epsilon \left[1, m_D^+\right] \\ e^{j\theta(i-1-m_D)}; & i \epsilon \left[m_D^+ + 1, m_D\right] \end{cases} \tag{26}$$

where

$$m_D^+ = [(m_D + 1)/2].$$

The particular form of the matrix $[D(\theta)]$ at it is given in (26) is due to the periodicity of the DFT. Now, given that $[W_F]$ is the DFT matrix of size $(m_D \times m_D)$, the vectors $[Z_{F_{\Gamma_S}}]$ and $[Z_{F_{\Gamma_R}}]$ are given in the following equations:

$$[Z_{F_{\Gamma_S}}] = [W_F]^{-1}[A_{\Gamma_S}] \tag{27}$$

$$[Z_{F_{\Gamma_R}}] = [W_F]^{-1}[A_{\Gamma_R}] \tag{28}$$

where vectors $[A_{\Gamma_S}]$ and $[A_{\Gamma_R}]$ are given in the following explicit expressions:

$$[A_{\Gamma_S}] = \begin{pmatrix} A_{\Gamma_{S0}} \\ A_{\Gamma_{S1}} \\ \vdots \\ \vdots \\ \vdots \\ A_{\Gamma_{S(N-1)}} \end{pmatrix}; \quad [A_{\Gamma_R}] = \begin{pmatrix} A_{\Gamma_{R0}} \\ A_{\Gamma_{R1}} \\ \vdots \\ \vdots \\ \vdots \\ A_{\Gamma_{R(N-1)}} \end{pmatrix}. \tag{29}$$

We should denote furthermore that the vectors $[A_{\Gamma_S}]$ and $[A_{\Gamma_R}]$ can be expressed in function of their DFT vectors $[Z_{\Gamma_S}]$ and $[Z_{\Gamma_R}]$ in the following expressions, respectively,

$$[Z_{\Gamma_S}] = [W_{\Gamma_S}]^{-1}[A_{\Gamma_S}] \tag{30}$$

$$[Z_{\Gamma_R}] = [W_{\Gamma_R}]^{-1}[A_{\Gamma_R}] \tag{31}$$

where

$$[W_{\Gamma_S}] = [W_{\Gamma_R}] = [U] \otimes \left[I_{d\left(\frac{m_D}{N}\right)}\right]. \tag{32}$$

Combining now (25), (27), (28), (30), and (31) leads to the following expression:

$$[Z_{\Gamma_R}] = [W_{\Gamma_R}]^{-1}[W_F][D(\theta)][W_F]^{-1}[W_{\Gamma_S}][Z_{\Gamma_S}]$$

$$[Z_{\Gamma_R}] = [Q][Z_{\Gamma_S}]. \tag{33}$$

The matrix $[D(\theta)]$ being diagonal; therefore, the matrix $[W_F][D(\theta)][W_F]^{-1}$ is circulant, which will lead furthermore to that in our case where $[W_{\Gamma_S}] = [W_{\Gamma_R}]$, the matrix $[Q] = [W_{\Gamma_R}]^{-1}[W_F][D(\theta)][W_F]^{-1}[W_{\Gamma_S}]$ is block diagonal.

The matrix $[Q]$ being block diagonal, each subvector $[Z_{\Gamma_{Ri}}]$ can be expressed as a function only of the corresponding vector $[Z_{\Gamma_{Si}}]$, thus leading from (23) and (24) to resolve $N$ independent coupled subsystems in the following form:

$$\begin{cases} [S_{ii}{}_{\Delta S}] \begin{bmatrix} Z_{Si} \\ Z_{\Gamma_{Si}} \end{bmatrix} = \begin{bmatrix} C_{Si} \\ C_{\Gamma_{Si}} \end{bmatrix} \\ [S_{ii}{}_{\Delta R}] \begin{bmatrix} Z_{Ri} \\ Z_{\Gamma_{Ri}} \end{bmatrix} = \begin{bmatrix} C_{Ri} \\ C_{\Gamma_{Ri}} \end{bmatrix} \\ [Z_{\Gamma_{Ri}}] = [Q_{ii}][Z_{\Gamma_{Si}}] \end{cases} ; \quad 0 \le i \le N-1. \tag{34}$$

We have then proved that the SFIM used to take into account the rotor motion does not affect the advantage of the exploitation of the geometrical periodicity for any rotation angle $\theta$ and leads always to $N$ reduced independent subsystems.

We should denote that to take into account the rotor motion while ensuring a model reduction by means of the exploitation of the geometrical periodicity, the matrices $[W_{\Gamma_S}]$ and $[W_{\Gamma_R}]$ should be equals. In fact, this condition is verified when the number of stator and rotor sections are equal. In fact, the choice of the same number of sections $N$ in both stator and rotor does not have any problem in the case of cylindrical rotor machine as in the case of SMPM, for example, since the rotor is without any saliency and thus the number $N$ of the machine periodical sections can be chosen equal to the number of stator teeth $N_S$, the elementary section presenting one stator tooth is effectively the smallest periodic section. However, in the case of salient pole rotor machines as for the cases of double-salient switched reluctance or buried permanent magnet machines, the rotor exhibits strong saliency: the machine consists now of $N_S$ stator teeth and $N_R$ rotor teeth (i.e., $N_R$ salient rotor poles). To ensure a geometrical periodicity, the number $N$ of the machine periodical or congruent sections must be chosen now using the greatest common divisor GCD as in the following equation [21]:

$$N = \text{GCD } (N_S, N_R). \tag{35}$$

### *C. Additional Contribution of the DFT on the Model Reduction by Looking on Their Properties*

As a summary, we have verified that the exploitation of the geometrical periodicity in some electromagnetic devices results in the transformation of a large system to be solved to several subsystems of small dimensions, thus leading to an acceleration in the computational time which is denoted $\gamma$. This was verified to be always true even when taking into account the continuous rotor motion using the SFIM.

Moreover, the normalized DFT has some particular characteristics such as the interdependence between the spectral components in the case of the DFT of real values. This type of interdependence will be studied in the following part, differentiating the two cases of sampling with an even or odd number $N$. In our case, the values undergoing the DFT are real numbers representing the nodal values of the magnetic potential. We can prove (see Appendix A) that if a vector $[Z]$ is the DFT of a real vector $[A]$ of dimension $N$, some components of $[Z]$ are interdependent. We can deduce that some subsystems in (34) do not need to be solved. For example, in the case where $N$ is even, the vector $[Z]$ can be given by its general representation form

$$[Z] = \begin{bmatrix} Z_0 \\ Z_{\frac{N}{2}-\alpha} \\ Z_{\frac{N}{2}} \\ Z_{\frac{N}{2}+\alpha} \end{bmatrix} \quad \text{where } \alpha \in [1; 2 \ldots; \frac{N}{2} - 1] \tag{36}$$

where

$$Z_{\frac{N}{2}+\alpha} = \overline{Z_{\frac{N}{2}-\alpha}}; \quad \alpha \in \left[1; 2 \ldots; \frac{N}{2} - 1\right]. \tag{37}$$

Only the $(N/2+1)$ subsystems associated with the vectors $Z_0$, $Z_{(N/2)-\alpha}$, and $Z_{(N/2)}$ are determined by solving (34). The other vectors $Z_{(N/2)+\alpha}$ will be deduced in a post-processing step using the simple conjugate relationship (37). Avoiding that the solving of all the $N$ subsystems, by solving only $(N/2-1)$ subsystems, increases, therefore, the acceleration in the computational time from $\gamma$ to $\gamma_p = \gamma \times (N/((N/2)+1))$.

However, in the case, where $N$ is odd, the general representation form of the vector [Z] is now

$$[Z] = \begin{bmatrix} Z_0 \\ Z_{\frac{N+1}{2}-\alpha} \\ Z_{\frac{N-1}{2}+\alpha} \end{bmatrix} \quad \text{where } \alpha \in \left[1; 2 \ldots; \frac{N}{2} - 1\right] \tag{38}$$

where

$$Z_{\frac{N-1}{2}+\alpha} = \overline{Z_{\frac{N+1}{2}-\alpha}}; \quad \alpha \in \left[1; 2 \ldots; \frac{N-1}{2}\right]. \tag{39}$$

Only the $(N+1)/2$ subsystems associated with the vectors $Z_0$ and $Z_{((N+1)/2)-\alpha}$ are determined by solving (34). The other vectors $Z_{((N-1)/2)+\alpha}$ will be deduced in a post-processing step using the simple conjugate relationship (39). We retrieve, therefore, the same property as the one pointed out in the case when $N$ is an even number and so the opportunity of speedup. However, the acceleration in the computational time when $N$ is odd is now quite different and it is given by $\gamma_p = \gamma \times \left(N/\left(\frac{N+1}{2}\right)\right)$.

### *D. Additional Contribution of the DFT on the Model Reduction by Looking on the Spectral Content of the Solution*

In several particular cases characterized by a regular distribution of the sources (currents and/or permanent magnets), one spectral harmonic of this distribution can be dominant, and thus a prevailing spectral harmonic of the solution predominantly governs the overall distribution of the full model solution. It seems profitable then to solve only the subsystem associated with the DFT component related to this prevailing harmonic. To benefit from this advantage, it is necessary, therefore, to determine the relationship between a given harmonic $k$ and a DFT component $Z_m$ of the vector $[Z]$.

In Appendix B, we have proven that the spectral information relating to the harmonic $k$ is represented by the component $m$ of the DFT vector such that the relation between $m$ and $k$ is described in the following expression:

$$k = |N \times l \pm m| \quad \text{where } l \in \mathbb{N}. \tag{40}$$

Knowing the prevailing harmonic $k$, then one can determine the dominant component $m$ of the DFT vector $[Z]$; the considered component $Z_m$will represent the spectral content of the harmonic $k$. Coming back now to the solution of the system (34): if we are in the case where the full model solution is governed by the harmonic $k$, thus giving the advantage of solving only and sufficiently in (34), the single FE subsystem linked to the components $[Z_{SSm}]$and $[Z_{RRm}]$. This will increase effectively the speedup to $\gamma_p = \gamma \times N$.

All these different cases will be treated in the following part on an application example of an SMPM.

## IV. Application Examples

The application example is a 9/8 SMPM (Fig. 4). It consists of nine stator teeth and eight rotor permanent magnets. Using the classical approach, there is no obvious magnetic symmetry and as a matter of fact the full geometry of the machine needs to be meshed. However, the rotor permeability (iron and magnet) is axisymmetric even though the residual magnetic flux density varies, but it does not alter the material characteristic, i.e., permeability and periodicity, as mentioned in Section II.

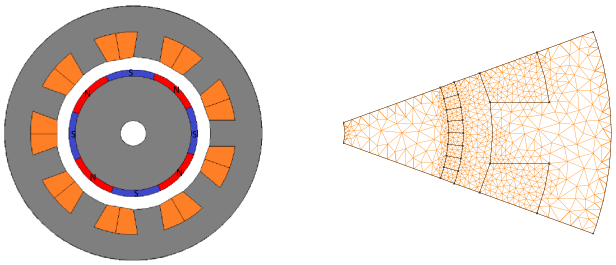

Fig. 4. Cylindrical SMPM 9/8 (left). Mesh of the 1/9 modeled section (right).

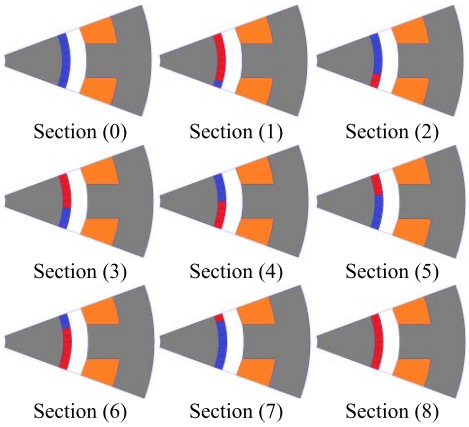


Fig. 5. Permanent magnet source distribution in the nine different sections.

In fact, the studied machine represents a stator saliency with $N_s = 9$ teeth and a cylindrical non-salient rotor. Therefore, the elementary periodic cell, as we have noticed in Section II, turns out to be only one stator tooth and representing 1/9 of the whole machine (Figs. 1 and 4). However, the rotor presents $N_a = 8$ permanent magnets; the symmetry, hence, is not consistent between the stator teeth and the rotor poles. To overcome this problem, the permanent magnets are subdivided each into $q$ portions, $d$ portions of which are modeled in the elementary section.$q$ and $d$ should verify the following equation:

$$d \times 9 = q \times 8 \tag{41}$$

In the simplest case, we can choose $d = 8$ and $q = 9$; each permanent magnet should be subdivided, therefore, into nine portions from which eight portions only are modeled in the elementary 1/9 machine section (Fig. 4). The residual magnetic flux density distribution in nine different sections is shown in Fig. 5, while the stator phases are left unloaded. We should denote that the 2-D spatial mesh of the elementary cell is made of $n = 625$ nodes and 1158 elements.

From the mesh of one cell, we have reconstructed a full FE model (reference) that we have compared to the reduced model. The exploitation of the geometrical periodicity makes it possible to switch effectively from the large FE system to nine independent subsystems. In our case, the transformation

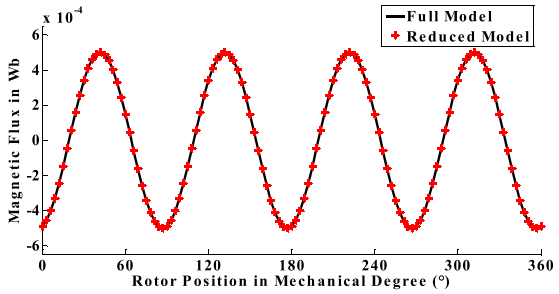


Fig. 6. Magnetic flux through a tooth coil calculated with the reference full model and the reduced model in the balanced regime.

from the real unknown values to the DFT values is given in the following relations

$$[Z_{SS}] = [W_S]^{-1}[A_{SS}] \quad \text{and} \quad [Z_{RR}] = [W_R]^{-1}[A_{RR}] \tag{42}$$

$$[Z_{SS}] = \begin{bmatrix} Z_{SS0} \\ Z_{SS1} \\ Z_{SS2} \\ Z_{SS3} \\ Z_{SS4} \\ Z_{SS5} \\ Z_{SS6} \\ Z_{SS7} \\ Z_{SS8} \end{bmatrix} \quad \text{and} \quad [Z_{RR}] = \begin{bmatrix} Z_{RR0} \\ Z_{RR1} \\ Z_{RR2} \\ Z_{RR3} \\ Z_{RR4} \\ Z_{RR5} \\ Z_{RR6} \\ Z_{RR7} \\ Z_{RR8} \end{bmatrix}. \tag{43}$$

Thanks to the particular properties of the DFT (see Section III-C), some spectral components are dependent. In our case, $N$ is odd; then, the components: $Z_{((N-1)/2)+\alpha} = \overline{Z_{((N+1)/2)-\alpha}}$ where $\alpha \in [1 : ((N-1)/2)]$. Therefore, if $N = 9$, the components $Z_{SS8}$, $Z_{SS7}$, $Z_{SS6}$, and $Z_{SS5}$ are linked to $Z_{SS1}$, $Z_{SS2}$, $Z_{SS3}$, and $Z_{SS4}$ and the corresponding subsystems can be not necessarily solved (same for $[Z_{RR}]$ components). The remaining five subsystems are solved, while the unknowns of the other subsystems will be deduced in a post-processing step. If we admit that the transformation into nine independent subsystems leads to a speedup of $\gamma$, the solving, hence, of five subsystems instead of nine will lead in addition to an advantage acceleration in the calculation time theoretically equal to $\gamma_p = \gamma \times 9/5$.

### A. Balanced Regime

The first application is the case of a balanced permanent magnet source distribution in the rotor, while the stator winding is kept unloaded. In fact, we have verified that the reduced model solution matches absolutely the one of the reference full model. The post-processing global quantity compared between both models is the magnetic flux flowing through a tooth coil (Fig. 6).

The local quantities are the flux line distribution (Fig. 7), the magnetic flux density (Fig. 8), and the magnetic potential calculated at the air-gap level in function of the angular position (Fig. 9). The flux lines, the flux density distributions, and the magnetic potential are calculated at a given rotor position, while the magnetic flux is calculated for a full rotor mechanical revolution. The speedup resulting from the transformation of the large system into nine independent subsystems has been

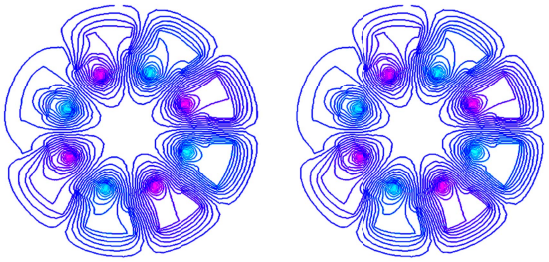

Fig. 7. Flux line distribution calculated with the reference full model (left) and the reduced model (right) in the balanced regime.

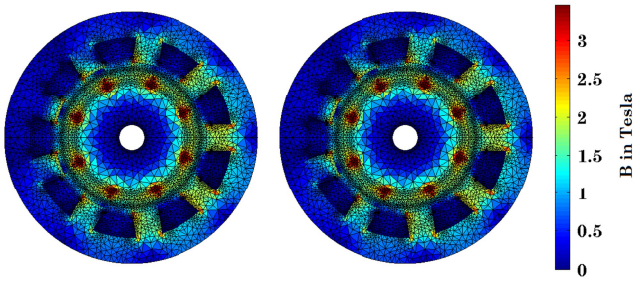


Fig. 8. Flux density distribution calculated with the reference full model (left) and the reduced model (right) in the balanced regime.

TABLE I
HARMONIC CONTENT OF EACH DFT COMPONENT

| | |
|---|---|
| $Z_0$ | $[\,l \times N\,]^+$ |
| $Z_1$ | $[l \times N-1, l \times N+1]^+$ |
| $Z_2$ | $[l \times N-2, l \times N+2]^+$ |
| $Z_3$ | $[l \times N-3, l \times N+3]^+$ |
| $Z_4$ | $[l \times N-4, l \times N+4]^+$ |

calculated; it is equal to $\gamma = 1.7$. Solving five instead of nine subsystems will lead moreover to a theoretical speedup of $\gamma = 1.7 \times \frac{9}{5} \approx 3$.

### B. Balanced Regime Considering Only $Z_4$

The distribution of the source in the rotor has a particular shape: it consists of four pairs of permanent magnets leading to a source distribution in such a way that the fourth harmonic is dominant. This can be verified by looking at the distribution of the magnetic potential calculated at the air-gap level and its spectral representation (Figs. 7 and 8). Since the fourth harmonic is dominant, the solution of the associated subsystem could be sufficient to obtain an acceptable accuracy compared to the full model (see Section III-D). According to (40), the spectral harmonics are projected into the DFT components as presented in Table I, where $l \epsilon \mathbb{N}$ and $[]^+$ represents the positive value. According to Table I, the spectral representation of the magnetic potential shown in Fig. 9 is plotted in Fig. 10 as a function of the harmonics and the associated DFT components.

The prevailing fourth harmonic corresponds to the case where $k = l \times N + 4 = 4$, $l = 0$, $m = 4$, and $N = 9$. As shown

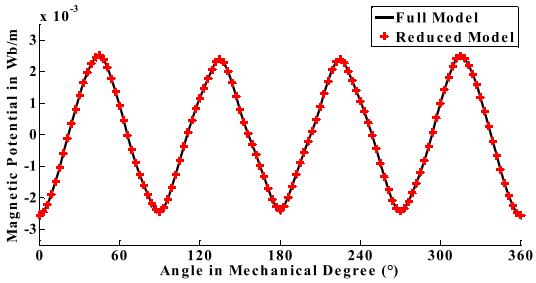


Fig. 9. Magnetic potential in the air gap in function of the angular position calculated with the reference full model and the reduced model in the balanced regime.

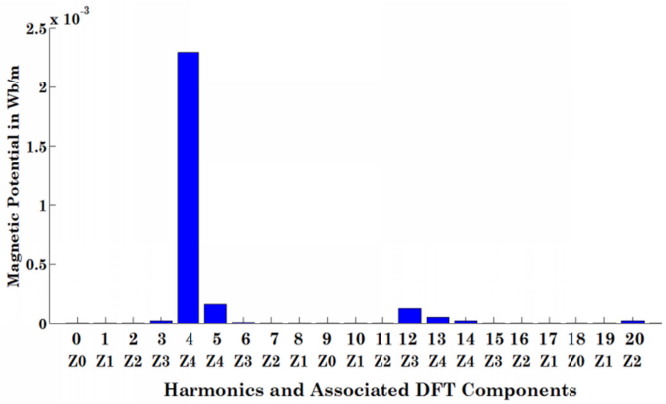


Fig. 10. Spectral representation of the magnetic potential distribution at the air-gap level in the balanced regime.

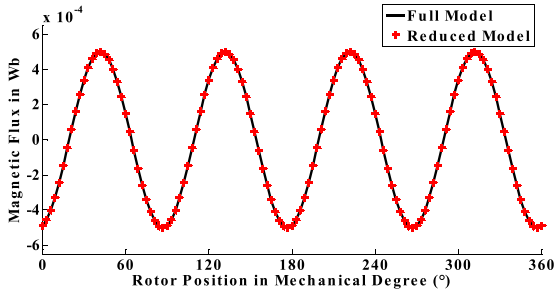


Fig. 11. Magnetic flux through a tooth coil calculated with the reference full model and the reduced model with only $Z_4$.

in Fig. 10, the fourth harmonic is associated with the DFT component $Z_4$. Therefore, the solution of the subsystem corresponding to $Z_4$ component seems to be sufficient to obtain an accepted accuracy. Generating now the global solution from the component $Z_4$ only, we have remarked that the model reduction solution matches very well the one of the reference full model.

The results are in agreement not only with respect to the global quantity of the magnetic flux (Fig. 11) where the error does not exceed 0.12% but also regarding the local ones (Figs. 12–14), but now with a slight low precision where the error considering the calculation of the magnetic potential in the air gap, for example, is about 5% (Fig. 14). Solving a single subsystem instead of nine allows an acceleration in time of calculation of order $\gamma_p = 9 \times 1.7 \approx 15$.

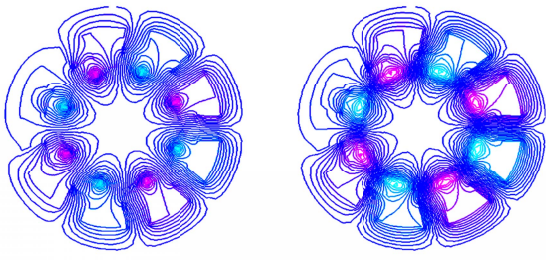

Fig. 12. Flux line distribution calculated with the reference full model (left) and the reduced model with only $Z_4$ (right).

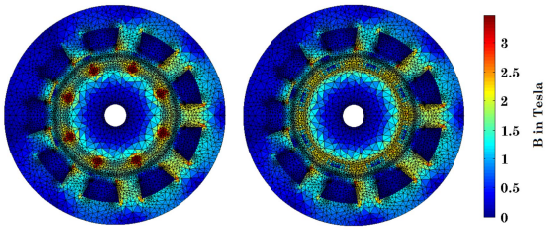


Fig. 13. Flux density distribution calculated with the reference full model (left) and the reduced model with only $Z_4$ (right).

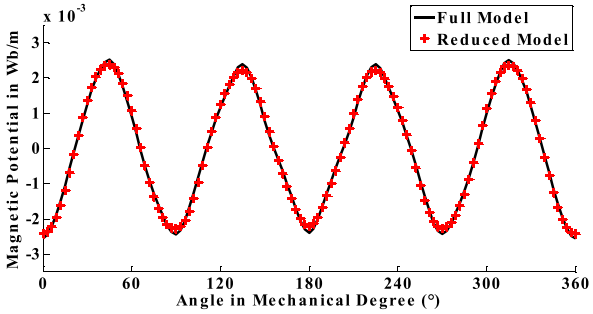


Fig. 14. Magnetic potential in the air gap in function of the angular position calculated with the reference full model and the reduced model with only $Z_4$.

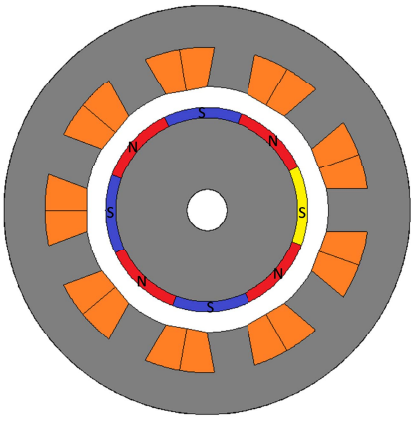


Fig. 15. 9/8 SMPM with a defect of a permanent magnet demagnetization in the rotor.

### *C. Unbalanced Regime With a Demagnetization of a Rotor Permanent Magnet*

In this section, we will study the case of unbalanced regimes that can be characterized by one of the following three cases:

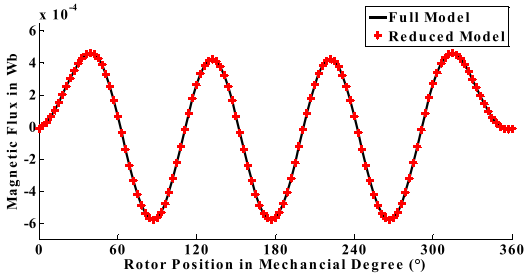


Fig. 16. Magnetic flux through a tooth coil calculated with the reference full model and the reduced model in the unbalanced regime.

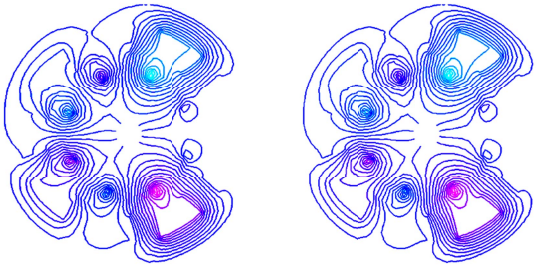

Fig. 17. Flux line distribution calculated with the reference full model (left) and the reduced model (right) in the unbalanced regime.

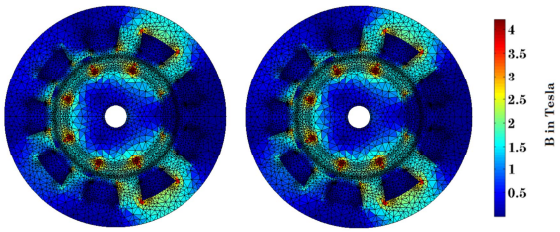


Fig. 18. Flux density distribution calculated with the reference full model (left) and the reduced model (right) in the unbalanced regime.

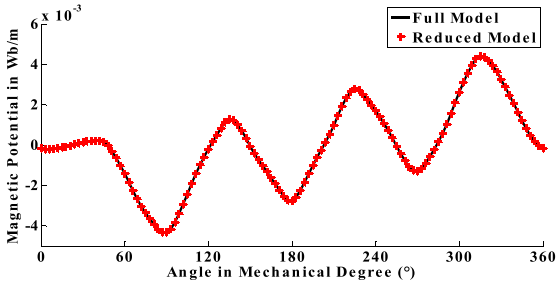


Fig. 19. Magnetic potential in the air gap in function of the angular position calculated with the reference full model and the reduced model in the unbalanced regime.

1) a demagnetization of a permanent magnet in the rotor;
2) a short circuit in the stator windings;
3) an unbalanced power supply to the stator.

In our case, since the stator is not loaded, we will study the case of an unbalanced regime characterized by a defect of demagnetization of a permanent magnet in the rotor (Fig. 15). This defect causes the rupture of the particular balanced distribution of the rotor source, and thus we are no longer in the case of a dominant harmonic: five of the nine subsystems must be solved. The solution is compared between the reference full model and the reduced model. They are in full agreement (Figs. 16–19) with an acceleration in computational time $\gamma_p = (9/5) \times 1.7 \approx 3$.

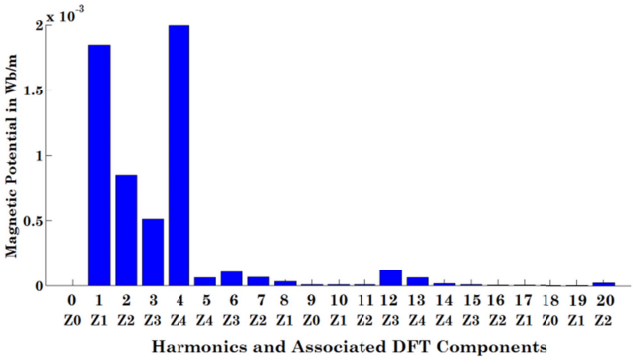


Fig. 20. Spectral representation of the magnetic potential distribution at the air-gap level in the unbalanced regime.

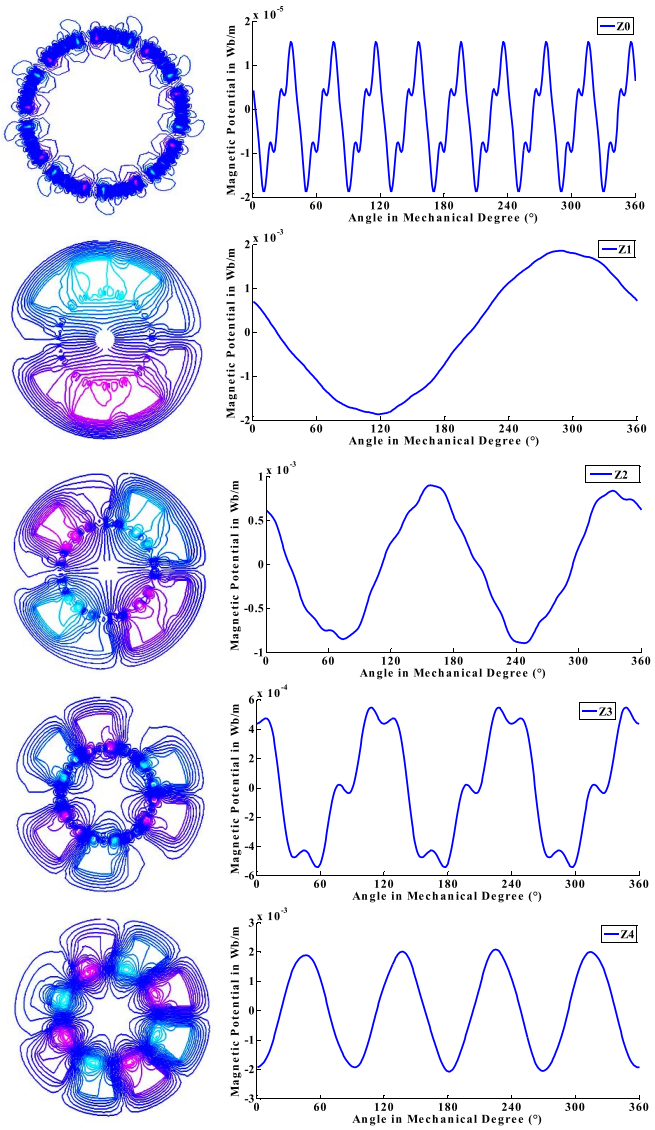


Fig. 21. Flux line distribution and air-gap magnetic potential calculated by means of different modes $Z_0$, $Z_1$, $Z_2$, $Z_3$, and $Z_4$ separately.

TABLE II
SPEEDUP IN THE FE COMPUTATIONAL TIME IN DIFFERENT CASES OF BALANCED AND UNBALANCED REGIMES

| Reduced-Model | | Speed-up |
|---|---|---|
| Balanced Regime | 9 subsystems $(Z_0, Z_1, Z_2, ..., Z_8)$ | $\gamma = 1.7$ |
| | 5 subsystems $(Z_0, Z_1, ..., Z_4)$ | $\gamma_p = 3.06$ |
| | 1 subsystem $(Z_4)$ | $\gamma_p = 15.3$ |
| Unbalanced Regime | 5 subsystems $(Z_0, Z_1, ..., Z_4)$ | $\gamma_p = 3.06$ |

The spectral representation of the magnetic potential distribution, as presented in Fig. 20, has shown that effectively there is not a single dominant harmonic, but many harmonics of important values.

Now, to see the contribution of each DFT component to the construction of the full problem solution, the solution is computed separately from different modes $Z_0$, $Z_1$, $Z_2$, $Z_3$, and $Z_4$. The corresponding flux line distribution and the magnetic potential calculated at the air-gap level are plotted in Fig. 21.

Finally, the acceleration in the computational time for the various problems treated previously is summarized in Table II.

## V. CONCLUSION

The presented approach based on the geometrical periodicity, and using the DFT, allows an efficient reduction of the FE model of an SMPM. Moreover, it was verified that the SFIM technique enables to model the continuous rotor movement while retaining the advantage of the geometrical periodicity.

The particular characteristics of the DFT allow additional acceleration in the computational time due to the inter-dependence between the harmonic components. Besides, a further acceleration can adequately take place in the case of a balanced regime where the solution distribution is governed by a single dominant spectral harmonic.

We should denote that these accelerations in the computational time have been obtained while even using a sequential computation. Nevertheless, an optimal speedup can be achieved, and that when using a parallel computation since the yielding reduced subsystems are effectively independent.

## APPENDIX

### A. Conjugate Relationship Between DFT Components

Assuming the case of a vector $X$ of dimension $N$ given in the following form:

$$[X] = [x_0 \quad x_1 \quad \cdots \quad x_m \quad \cdots \quad x_{(N-1)}]^T. \tag{44}$$

The DFT vector $[Z]$ of $[X]$ will be given in the following expression using the inverse DFT matrix $[U]^{-1}$:

$$[Z] = [U]^{-1}[X] = [Z_0 \quad Z_1 \quad \cdots Z_m \quad \cdots \quad Z_{N-1}]^T \tag{45}$$

where the entries of $[U]^{-1}$ are given by

$$U^{-1}(l,c) = \frac{1}{\sqrt{N}} e^{-j\times\frac{2\pi}{N}\times(l-1)\times(c-1)} \quad 1 \le l \le N \text{ and } 1 \le c \le N. \tag{46}$$

From (45) and (46), the general term $Z_m$ of the vector $[Z]$ will be given, therefore, in the following expression:

$$Z_m = \sum_{n=0}^{N-1} x_n e^{-j\times\frac{2\pi}{N}\times m\times n}. \tag{47}$$

Let us first suppose the case where $N$, the number of samples is even; then, the vector $[Z]$ can be given by its general representation form

$$[Z] = \begin{bmatrix} Z_0 \\ Z_{\frac{N}{2}-\alpha} \\ Z_{\frac{N}{2}} \\ Z_{\frac{N}{2}+\alpha} \end{bmatrix} \quad \text{where } \alpha \in \left[1; 2 \ldots; \frac{N}{2} - 1\right]. \tag{48}$$

Based on (47), the expressions of both general terms $Z_{(N/2)-\alpha}$ and $Z_{(N/2)+\alpha}$ will be given by

$$Z_{\frac{N}{2}-\alpha} = \sum_{n=0}^{N-1} x_n e^{-j\times\pi\times n} \times e^{j\times\frac{2\pi}{N}\times\alpha\times n} \tag{49}$$

$$Z_{\frac{N}{2}+\alpha} = \sum_{n=0}^{N-1} x_n e^{-j\times\pi\times n} \times e^{-j\times\frac{2\pi}{N}\times\alpha\times n}. \tag{50}$$

With $n$ being an integer which takes the values $1, 2, \ldots, N-1$, the term $e^{-j\times\pi\times n}$ is then a real number that can take the values 1 or $-1$. We can then deduce, from (49) to (50), that $Z_{(N/2)+\alpha}$ and $Z_{(N/2)-\alpha}$ are conjugate

$$Z_{\frac{N}{2}+\alpha} = \overline{Z_{\frac{N}{2}-\alpha}}; \quad \alpha \in \left[1; 2 \ldots; \frac{N}{2} - 1\right]. \tag{51}$$

In the other case, where the sampling number $N$ is odd, the vector $[Z]$ can be given its general representation form

$$[Z] = \begin{bmatrix} Z_0 \\ Z_{\frac{N+1}{2}-\alpha} \\ Z_{\frac{N-1}{2}+\alpha} \end{bmatrix} \quad \text{where } \alpha \in \left[1; 2 \ldots; \frac{N}{2} - 1\right]. \tag{52}$$

In the same way, based on (47), the expressions of both general terms $Z_{((N+1)/2)-\alpha}$ and $Z_{((N-1)/2)+\alpha}$ will be given by

$$Z_{\frac{N+1}{2}-\alpha} = \sum_{n=0}^{N-1} x_n e^{-j\times\pi\times n} \times e^{-j\times\frac{\pi}{N}\times(1-2\alpha)\times n} \tag{53}$$

$$Z_{\frac{N-1}{2}+\alpha} = \sum_{n=0}^{N-1} x_n e^{-j\times\pi\times n} \times e^{j\times\frac{\pi}{N}\times(1-2\alpha)\times n}. \tag{54}$$

We can then deduce from (53) and (54) that $Z_{((N+1)/2)-\alpha}$ and $Z_{((N-1)/2)+\alpha}$ are conjugate

$$Z_{\frac{N-1}{2}+\alpha} = \overline{Z_{\frac{N+1}{2}-\alpha}}; \quad \alpha \in \left[1; 2 \ldots; \frac{N-1}{2}\right]. \tag{55}$$

### B. Spectral Content of DFT Components

Let us consider the case of a signal $x(t)$ representing a sinusoidal function of frequency $kf$ corresponding to the $k$th harmonic of a reference signal of frequency $f$. When this given $k$th harmonic signal whose mathematical representation is $x(t) = A_k \sin(k2\pi ft)$ and is discretizing through a sampling frequency $F_s = N \times f$, the sampling vector consisting of the $N$ samples will be given in the following form:

$$[X] = \begin{bmatrix} 0 \\ A_k \sin(k2\pi/N) \\ \vdots \\ A_k \sin(k2\pi/N \times m) \\ \vdots \\ A_k \sin(k2\pi/N \times (N-1)) \end{bmatrix}. \quad (56)$$

Performing now in a following step, the DFT of the vector $[X]$ which leads to the vector $[Z] = \left[U^{-1}\right][X]$ whose general term, using (47), is given in the following expression:

$$Z_m = \sum_{n=0}^{N-1} \frac{A_k}{2j\sqrt{N}} \left[ e^{\frac{j\times 2\pi\times(k-m)}{N}\times n} - e^{-\frac{j\times 2\pi\times(k+m)}{N}\times n} \right]. \quad (57)$$

Indeed, terms $e^{((j\times 2\pi\times(k-m))/N)}$ and $e^{-((j\times 2\pi\times(k+m))/N)}$ represent, respectively, the $N$th roots of the complex numbers: $e^{j\times 2\pi\times(k-m)}$ and $e^{-j\times 2\pi\times(k+m)}$. Since $(k-m) \in \mathbb{Z}$ and $(k+m) \in \mathbb{Z}$, both complex numbers $e^{j\times 2\pi\times(k-m)}$ and $e^{-j\times 2\pi\times(k+m)}$ are thus equal to 1, and therefore both series in (57) will be equal to zeros since they represent in fact the sum of the $N$th roots of unity. However, one of these sums will be non-zero if there exists an integer $l$ such that

$$k \pm m = N \times l. \quad (58)$$

In the excepted cases presented by the relation (58), $e^{((j\times 2\pi\times(k-m))/N)\times n}$ or $e^{-((j\times 2\pi\times(k+m))/N)\times n}$ will be equal to 1 regardless the value of $n$; $Z_m$ will be not equal to zero, and it will include, therefore, the spectral information on the harmonic $k$.

## REFERENCES


[1] N. Ida and J. P. A. Bastos, *Electromagnetics and Calculation of Fields*. New York, NY, USA: Springer, 1997.

[2] C. A. Brebbia, *The Boundary Element Method for Engineers*. New York, NY, USA: Wiley, 1978.

[3] R. V. Sabariego and P. Dular, "A perturbation approach for the modeling of eddy current nondestructive testing problems with differential probes," *IEEE Trans. Magn.*, vol. 43, no. 4, pp. 1289–1292, Apr. 2007.

[4] M. Al Eit, P. Dular, F. Bouillault, C. Marchand, and G. Krebs, "Perturbation finite element method for efficient copper losses calculation in switched reluctance machines," *IEEE Trans. Magn.*, vol. 53, no. 6, pp. 1–4, Jun. 2017.

[5] A. Chatterjee, "An introduction to the proper orthogonal decomposition," *Current Sci.*, vol. 78, no. 7, pp. 808–817, 2000.

[6] M. Al Eit, F. Bouillault, C. Marchand, and G. Krebs, "Model-order nonlinear subspace reduction of electric machines by means of POD and DEI methods for copper losses calculation," *Int. J. Numer. Model.*, vol. 31, no. 2, p. e2274, 2017.

[7] M. Rosu *et al.*, "Basics of electrical machines design and manufacturing tolerances," in *Multiphysics Simulation by Design for Electrical Machines, Power Electronics, and Drives, One*, vol. 1. New York, NY, USA: Wiley, 2018.

[8] M. Siami, D. A. Khaburi, M. Rivera, and J. Rodríguez, "A computationally efficient lookup table based FCS-MPC for PMSM drives fed by matrix converters," *IEEE Trans. Ind. Electron.*, vol. 64, no. 10, pp. 7645–7654, Oct. 2017.

[9] A. Bossavit, "The exploitation of geometrical symmetry in 3-D eddy-currents computation," *IEEE Trans. Magn.*, vol. MAG-21, no. 6, pp. 2307–2309, Nov. 1985.

[10] J. Lobry and C. Broche, "Exploitation of the geometrical symmetry in the boundary element method with the group representation theory," *IEEE Trans. Magn.*, vol. 30, no. 1, pp. 118–123, Jan. 1994.

[11] J. Lobry, J. Trecat, and C. Broche, "Symmetry and TLM method in nonlinear magnetostatics," *IEEE Trans. Magn.*, vol. 32, no. 3, pp. 702–705, May 1996.

[12] M. Hamermesh, *Group Theory and its Application to Physical Problems*. Boston, MA, USA: Addison-Wesley, 1962.

[13] L. Jansens and M. Boon, *Theory of Finite Groups. Applications in Physics*. Amsterdam, The Netherlands: North Holland, 1967.

[14] P. J. Davis, *Circulant Matrices*. New York, NY, USA: Chelsea House Publishing, 1994.

[15] B. Dickinson and K. Steiglitz, "Eigenvectors and functions of the discrete Fourier transform," *IEEE Trans. Acoust., Speech, Signal Process.*, vol. ASSP-30, no. 1, pp. 25–31, Feb. 1982.

[16] M. Chiampi, D. Chiarabaglio, and M. Repetto, "A Jiles–Atherton and fixed-point combined technique for time periodic magnetic field problems with hysteresis," *IEEE Trans. Magn.*, vol. 31, no. 6, pp. 4306–4311, Nov. 1995.

[17] H. D. Gersem and T. Weiland, "Harmonic weighting functions at the sliding interface of a finite-element machine model incorporating angular displacement," *IEEE Trans. Magn.*, vol. 40, no. 2, pp. 545–548, Mar. 2004.

[18] L. Montier, S. Clenet, T. Henneron, and B. Goursaud, "Rotation movement based on the spatial Fourier interpolation method (SFIM)," *IEEE Trans. Magn.*, vol. 53, no. 6, pp. 1–4, Jun. 2017.

[19] T. W. Preston, A. B. J. Reece, and P. S. Sangha, "Induction motor analysis by time-stepping techniques," *IEEE Trans. Magn.*, vol. MAG-24, no. 1, pp. 471–474, Jan. 1988.

[20] B. Olson, S. Shaw, C. Shi, C. Pierre, and R. Parker, "Circulant matrices and their application to vibration analysis," *Appl. Mech. Rev., Amer. Soc. Mech. Eng.*, vol. 66, no. 4, p. 040803, 2014.

[21] N. Larsen, A. Gensior, and P. Hein, "Torque ripple reduction based on current control for a flux switching permanent magnet machine," in *Proc. Int. Symp. Power Electron. Elect. Drives, Autom. Motion*, Sorrento, Italy, Jun. 2012, pp. 712–717.